2026 IEEE International Conference on Robotics and Automation (ICRA 2026)
June 1-5, 2026. Vienna, Austria

A Hierarchical Adaptive Controller with Configurable Joint Torque Constraints for Flexible LIMS Elbow Cable-Driven Mechanism

Bin Liang[1], Yibo Gao*[1], Yang Deng[1], Kai Gong[1], Xudong Zheng[1], Zhili Hou[1], Weining Lu[2], and Chunting Jiao[1]

***Abstract*— Cable-driven mechanisms (CDMs) provide enhanced safety for human interaction thanks to their lightweight design and inherent compliance. However, designing high-performance tracking controller for CDMs is challenging due to the complex dynamics introduced by cables' flexibility. Existing works studied improving tracking performance for CDMs, but joint torque constraints are rarely considered, which may cause cable slack and bring additional uncertainties into system dynamics. Besides, most works modeled the actuator-to-joint transmission as a linear torsional spring, making it nontrivial to implement the controllers to CDMs with complex transmission mechanical design. To further enhance the compliance and safety and mitigate cable slackness of CDMs, we propose a novel hierarchical adaptive controller with configurable joint torque constraints for LIMS (Low Inertia Manipulator with high Stiffness and Strength) elbow CDM. The controller consists of an anti-windup adaptive joint control loop and a decoupled cable deformation control loop, which can achieve safe and compliant physical interaction without using torque/tension sensors or force/torque observers. Finally, the controller's stability is analyzed, and its capabilities in accuracy, safety, and compliance are validated via comprehensive experiments compared to the other two baseline controllers.**

I. Introduction

Cable-driven mechanisms enhance safety for human interaction through the low-link inertia and mass, achieved by placing actuators at the base [1], [2]. These mechanisms also provide inherent mechanical compliance via cable flexibility, making them particularly promising for applications in collaborative robots. The antagonistic design is common in CDMs where the revolute joint's bidirectional motion is actuated by a pair of flexible cables. The design is inspired by human muscle where one cable pulls the joint while the other releases during the motion. Moreover, LIMS elbow CDM in [2] employs a unique tension-amplification design which significantly increases joint stiffness and improve actuator-to-joint torque bandwidth.

One fundamental challenge of joint tracking control for CDMs is introduced by the cables' flexibility. The actuator-to-joint torque bandwidth is thus inevitably decreased [2], which complicates the design of joint tracking controller with high accuracy and low response time. Similar to CDMs, actuator-to-joint transmission is also flexible and it could be modeled as a torsional linear spring in the system dynamics model. Extensive research on tracking control of flexible-joint manipulator has been conducted [3]–[5].

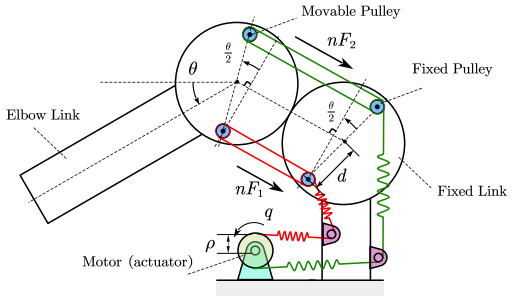

Fig. 1: A simplified diagram of LIMS elbow CDM [2].

CDMs also have distinct complexity in its dynamics compared with flexible-joint manipulators, which poses another challenge for tracking control. For example, cable slack could introduce state-dependent non-smooth elements into dynamics of CDMs: for antagonistic design, one cable would be slack when the other's tension is above a certain level [1]. In [6], the cable mechanics including internal friction and hysteresis are modeled to improve joint position tracking accuracy. Researchers have studied model-based control algorithms for CDMs [7], [8] based on Kalman filters and sliding mode control. Model-free methods including neural-network, time-delay estimation, adaptive control, etc. are also studied to address robustness issue under uncertainties in CDMs' dynamics brought by cables' felxibility [9]–[12].

While most researchers focus on improving the motion control performance for CDMs, few works have considered joint torque constraints for CDMs with antagonistic design, which would compromise safety interactions and cause cable slack. Though works of parallel CDMs impose tension constraints with several algorithms in [13], the mechanical design is different with the antagonistic design in [1], [2] which does not have redundant actuators to control the tension for each cable. In addition, most existing literature modeled the actuator-to-joint dynamics as a linear torsional spring, which is different with CDMs like LIMS where mapping from cable tensions to joint torque is nonlinear [2]. By introducing configurable joint torque constraints, the safety and compliance of CDMs could be further enhanced and cable slack phenomenon could also be alleviated. Since the joint actuated torque depends on the difference of cable tensions and cable deformation could be

This work is supported by the National Natural Science Foundation of China. (grant number: 62573252).

[1] Bin Liang, Yibo Gao, Yang Deng, Kai Gong, Xudong Zheng, Zhili Hou, and Chunting Jiao are with the Qiyuan Lab, Beijing, 100194, China.
[2] Weining Lu is with the Beijing National Research Center for Information Science and Technology, Beijing, 100084, China.
Corresponding author: Yibo Gao, email:gaoyibo@qiyuanlab.com.

estimated by joint and actuator positions, it is possible to introduce configurable joint torque constraints by bounding cable deformation during the control process. Motivated by this idea, we propose a novel hierarchical adaptive controller design which includes an anti-windup adaptive joint-loop and a cable-loop to control cable deformations using motor and joint positions feedback.

Unlike existing works, we propose a tracking controller with configurable joint torque constraints for LIMS elbow CDM. The CDM's nonlinear mapping between cable tensions and joint torque brings in extra complexity in system dynamics and challenges for the controller implementation in practice. The main contributions of this paper include: 1) a stability analysis is provided for the proposed controller, which relaxes the assumption in [3] that joint-loop controller should always have continuous second derivatives; 2) the inherent compliance of LIMS elbow CDM is further enhanced by introducing the configurable joint torque constraints; 3) cable slack phenomenon is mitigated by bounding cable deformation in the cable loop. Comprehensive experiments including tracking with varying load conditions, tracking of fast or abrupt trajectories, and compliance motion have been conducted to verify the proposed controller's features.

The paper is organized as follows. Section II introduces the setup and dynamic model of LIMS elbow mechanism and presents the control objective. In Section III, anti-windup adaptive tracking controller proposed in [14] is first reviewed, and then our proposed controller is presented with a stability analysis. Section IV presents the experimental results of the proposed controller and a modified controller for comparison. In Section V, we conclude this paper with the summary and future work.

II. System Description And Objective Statement

LIMS is introduced in [2] and a unique tension-amplification design is presented. The mechanism could be simplified as four parts: a motor, two cables, one fixed link and one movable elbow link. The basic diagram for the mechanism is shown in Figure 1, where θ is the position of the elbow joint, d is the half of the distance between the centers of two fixed or movable pulleys, n is the number of straight cable segments between each fixed and movable pulley pair, ρ is the radius of the drum fixed to the motor, q is the motor's position, and F_1, F_2 are tensions of the two individual cables. The bidirectional motion of the elbow link is driven by the motor via the pair of cables. The red and green lines represent two independent cables. Each cable is winded around the fixed pulley and movable pulley pair, which forms "block and tackle". The circular part of the elbow link has the motion constraint such that it always undergoes pure rolling motion around the circular surface of the fixed link.

For the system in Figure 1, the zero position of motor is where $\theta = 0$ and the tensions of two cables are equal. Based on the cable kinematics presented in [2], the deformation of each cable due to the movement of the motor and joint is

$$l = \rho \left(q - f_{kin} \left(\theta \right) \right) \tag{1}$$

where $f_{kin}\left(\theta\right)$ is the function describing the kinematics relationship between the motor and joint if the cables are considered as rigid. In Figure 1 and according to [2], the ideal kinematics is $f_{kin}(\theta) = \frac{1}{\rho}\left(2nd \sin\frac{\theta}{2}\right)$. But in practice this may not be accurate enough to model the true kinematics due to the complex cable routing in the real mechanism.

In this paper, we assume cables would become slack when its tension is under a certain level. Hence, we model the mechanics property of cables based on Hooke's Law as

$$\begin{aligned} F_1 &= F_p + kl \quad \text{if } l \geq \left(F_0 - F_p\right)/k \\ F_2 &= F_p - kl \quad \text{if } l \leq -\left(F_0 - F_p\right)/k \ . \end{aligned} \tag{2}$$

where F_p, F_0 are cable pretension and the tension level under which cable slack could not be tolerated, k is the stiffness. F_1 and F_2 are not modeled when $l \notin \left[-\frac{1}{k}\left(F_p - F_0\right), \frac{1}{k}\left(F_p - F_0\right)\right]$. Cable routings would change when being slack, which brings in uncertainties in $f_{kin}(\theta)$. Therefore, the complexity of cable mechanics and kinematics in this case would increase significantly. By Lagrangian mechanics, we could obtain the following dynamic model for the elbow mechanism

$$\begin{aligned} J(\theta)\ddot{\theta} + \left(B_0 + C(\dot{\theta}, \theta)\right)\dot{\theta} + g(\theta) &= -(\partial_\theta l)(F_1 - F_2) \\ J_\rho \ddot{q} &= u - \rho\left(F_1 - F_2\right) \end{aligned} \tag{3}$$

where $\partial_\theta l = \frac{\partial l}{\partial \theta}$ and $J(\theta), C(\dot{\theta}, \theta), g(\theta)$ are inertia, Coriolis/centrifugal, and gravitational functions for the elbow link, respectively. The specific expressions are presented in Appendix. B_0 is the damping term which is caused by frictions, J_ρ is motor's inertia, and u is the control torque for the motor.

We use τ to denote joint torque caused by cable tensions in (3). By (2), when neither of the cables is slack,

$$\tau(\theta, q) = -(\partial_\theta l)\left(2kl\right). \tag{4}$$

In this paper, the control objective is to design a controller u such that the tracking error $\tilde{\theta} = \theta - \theta_d$ would asymptotically converge to zero and joint torque constraint is satisfied: $\tau\left(t\right) \in [-\tau_m, \tau_m]$, where $\tau_m > 0$ is a bound chosen by users to achieve safety interactions.

To help the analysis of stability for the proposed controller, the following assumptions are used in this paper.

Assumption 1. *The desired joint trajectory $\theta_d(t)$ is at least four times continuously differentiable.*

Assumption 2. *$|\tau_d| < \tau_m$ for all $t > 0$, where τ_d is the desired joint torque defined as follows:*

$$\tau_d = J(\theta_d)\ddot{\theta}_d + (B_0 + C(\dot{\theta}_d, \theta_d))\dot{\theta}_d + g(\theta_d). \tag{5}$$

Assumption 3. *$\theta \in \left[-\frac{\pi}{2}, \frac{\pi}{2}\right]$ throughout the control process.*

Assumption 4. *The third-order derivative of $f_{kin}(\theta)$ with respect to θ is continuous.*

Assumption 1 is a standard assumption for tracking control of flexible-joint manipulators, Assumption 2 is used to guarantee $|\tau| < \tau_d$ when $\theta(t) = \theta_d(t)$, and Assumption 3 is necessary for not damaging the experimental mechanism. Assumption 4 holds for most CDMs. $f_{kin}(\theta)$ is smooth in the ideal case when $f_{kin}(\theta) = \frac{1}{\rho}\left(2nd\sin\frac{\theta}{2}\right)$.

III. The Hierarchical Adaptive Controller with Configurable Joint Torque Constraints

A. Review of Anti-windup Adaptive Tracking Control for Manipulators

The controller proposed in [14] could be applied to the dynamic model (3) if τ is the constrained controller input:

$$J(\theta)\ddot{\theta} + \left(B_0 + C(\dot{\theta},\theta)\right)\dot{\theta} + g(\theta) = \sigma(\tau_R). \tag{6}$$

where τ_R is the joint control input, and $\sigma(\tau_R)$ is the saturation function of control input which is defined as

$$\sigma(\tau_R) = \begin{cases} \tau_R & \text{if } \tau_R \in [-\tau_m, \tau_m] \\ \tau_m & \text{if } \tau_R \in (\tau_m\ , +\infty) \\ -\tau_m & \text{if } \tau_R \in (-\infty\ , -\tau_m)\,. \end{cases} \tag{7}$$

The saturation function limits joint torque to the user specified bound $\pm\tau_m$. The adaptive anti-windup controller is designed to achieve tracking of joint trajectories for (6) with input saturation. The controller has the following form

$$\tau_R = -A\tilde{\theta} - B\dot{\tilde{\theta}} + Y\left(\theta_d, \dot{\theta}_d, \dot{\theta}_d, \ddot{\theta}_d\right)\hat{p} \tag{8}$$

where A and B are positive constants, $\hat{p}$ is the estimation of unknown dynamic parameters p, and Y is a matrix excluding unknown dynamic parameters such that $Y\left(\theta,\dot{\theta},\dot{\theta},\ddot{\theta}\right)p$ is equal to the left-hand side of (6). The expression of Y is shown in Appendix. The updating law for $\hat{p}$ is

$$\begin{aligned} \hat{p} &= -P^1\int_0^t Y\left(\theta_d,\dot{\theta}_d,\dot{\theta}_d,\ddot{\theta}_d\right)^T\left(\bar{y}_1 + \alpha\bar{y}_2\right)dt, \\ \bar{y}_1 &= \dot{\tilde{\theta}} \quad \text{if } \dot{\tilde{\theta}}\psi(\tau_R) \geq 0 \\ \bar{y}_1 &= 0 \quad \text{if } \dot{\tilde{\theta}}\psi(\tau_R) < 0 \\ \bar{y}_2 &= s\left(\tilde{\theta}\right) \quad \text{if } s\left(\tilde{\theta}\right)\psi(\tau_R) \geq 0 \\ \bar{y}_2 &= 0 \quad \text{if } s\left(\tilde{\theta}\right)\psi(\tau_R) < 0 \end{aligned} \tag{9}$$

where $\psi(\tau_R) = \tau_R - \sigma(\tau_R)$, $s(.)$ is a smooth saturation function, and α is a positive constant. Note that the updating law of $\hat{p}$ has four different cases in total. The switching rule is particularly useful to guarantee the tracking performance under input saturation. Next, we state remark 1 of the main theorem of [14] and omit the assumptions and the proof for brevity.

Corollary of the main theorem [14]. *If the assumptions in [14] hold, with the anti-windup adaptive controller* (8) *and* (9)*, the tracking error $\tilde{\theta}$ of the closed-loop system would globally asymptotically converge to zero.*

B. Design and Stability of The Proposed Controller

The proposed controller incorporates the idea of the adaptive anti-windup controller in [14] and the decoupling control for flexible-joint manipulator in [3]. By (2) and (3), the dynamic model when cable is not slack could be rewritten as

$$J(\theta)\ddot{\theta} + \left(B_0 + C(\dot{\theta},\theta)\right)\dot{\theta} + g(\theta) = (-\partial_\theta l)(2kl) \tag{10a}$$

$$J_\rho\ddot{q} = u - \rho(2kl)\,. \tag{10b}$$

The proposed controller is

$$u = \rho(2kl) - K_1\tilde{q} - K_2\dot{\tilde{q}} + J_\rho\ddot{q}_\mathrm{d} \tag{11}$$

where $\tilde{q} = q - q_d$ and

$$q_d = \frac{1}{\rho}\left(\frac{\sigma(\tau_R)}{2k(-\partial_\theta l)}\right) + f_{kin}(\theta)\,. \tag{12}$$

τ_R is same as in (8) and (9). The saturation function $\sigma(.)$ in (7) is used. Substitute q in (1) with $\tilde{q} + q_d$ and τ in (10a) becomes

$$\tau = (-\partial_\theta l)(2kl) = \sigma(\tau_R) + (-\partial_\theta l)\,2k\rho\tilde{q} \tag{13}$$

The second term of τ could be considered as disturbance and τ would converge to $\sigma(\tau_R)$ if $\tilde{q}$ converges to 0. We refer to controller (11) as cable-loop controller since it essentially controls the deformation of the cable to produce desired joint torque $\sigma(\tau_R)$. We call τ_R as joint-loop controller and the overall hierarchical controller structure is shown in Figure 2.

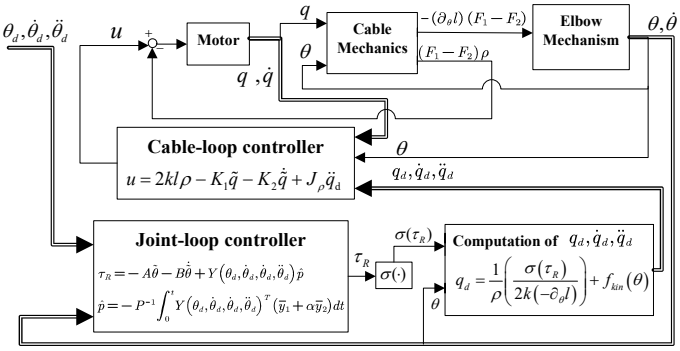

Fig. 2: The control diagram of the proposed controller.

The closed-loop system could be obtained by substituting controller (11) into (10b):

$$J\ddot{\theta} + (B_0 + C)\dot{\theta} + g = \sigma(\tau_R) + (-\partial_\theta l)(2k\rho\tilde{q}) \tag{14a}$$

$$J_\rho\ddot{\tilde{q}} + K_2\dot{\tilde{q}} + K_1\tilde{q} = 0\,. \tag{14b}$$

Motor error dynamics in (14b) is decoupled from the joint error dynamics and it is an exponentially stable system when K_1, $K_2 > 0$ and $\dot{q}_d, \ddot{q}_d$ are continuous. If $\tilde{q} \to 0$, $\tau \to \sigma(\tau_R)$ and the stability of $\tilde{\theta}$ is already discussed in the corollary of III-A if $\tau = \sigma(\tau_R)$. However, $\dot{q}_d, \ddot{q}_d$ may not exist sometimes since $\sigma(\tau_R)$ is not differentiable at $\tau_R = \pm\tau_m$. Therefore, it is not trivial to prove $\tilde{q} \to 0$.

By Assumption 1 and 4, $\dot{q}_d, \ddot{q}_d$ are continuous if and only if $\dot{\sigma}(\tau_R)$,$\ddot{\sigma}(\tau_R)$ are continuous. The only case when $\dot{\sigma}(\tau_R), \ddot{\sigma}(\tau_R)$ do not exist is when the proposed controller switches between $\psi(\tau_R) \neq 0$ and $\psi(\tau_R) = 0$. The argument is analyzed in the following. When $\psi(\tau_R) = 0$, $\sigma(\tau_R) = \tau_R$ and $\dot{\sigma}(\tau_R), \ddot{\sigma}(\tau_R)$ are continuous by (9), Assumption 1, and 4. When $\psi(\tau_R) \neq 0$, $\sigma(\tau_R) = \tau_m$ or $-\tau_m$ always holds no matter how (9) switches. Thus, $\dot{\sigma}(\tau_R) = 0$ in this case. If switching between $\psi(\tau_R) = 0$ and $\psi(\tau_R) \neq 0$ happens, $\dot{\sigma}(\tau_R)$ and $\ddot{\sigma}(\tau_R)$ do not exist because $\sigma(\tau_R)$ is not differentiable at $\tau_R = \pm\tau_m$. For simplicity of notation, we define $\dot{q}_d, \ddot{q}_d$ to be zero each time such switching happens.

A simple case to prove $\tilde{q} \to 0$ is when $\psi(\tau_R) = 0$ always holds after a finite period as shown by the blue signal of Figure 3. This is possible in practice when Assumption 2 holds. From the previous analysis, $\dot{q}_d, \ddot{q}_d$ are continuous when $\psi(\tau_R) = 0$. By choosing $K_1, K_2 > 0$ in the cable-loop controller (11), $\tilde{q}$ would be asymptotically stable.

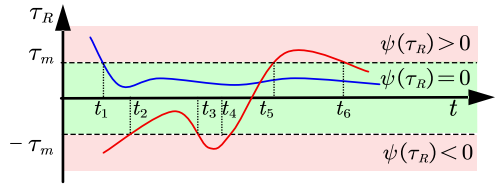

Fig. 3: Two examples of τ_R. Blue: $\psi(\tau_R) = 0$ holds after finite time. Red: τ_R switches between $\psi(\tau_R) = 0$, $\psi(\tau_R) \neq 0$.

In general, $\psi(\tau_R) = 0$ may not always hold after finite time as shown by the red signal of Figure 3. Nonetheless, the boundness of $\tilde{\theta}$ could be analyzed if the following assumption is made.

Assumption 5. *For the closed-loop system* (14)*, the joint-loop controller is free of Zeno behavior when switching between* $\psi(\tau_R) = 0$ *and* $\psi(\tau_R) \neq 0$.

The assumption is much weaker than requiring $\psi(\tau_R) = 0$ after finite time. If the above assumption holds, infinitely fast switching would not happen and there exists a minimum dwell time between every two consecutive discontinuities of $\dot{q}_d, \ddot{q}_d$. If we could design K_1, K_2 in the motor controller to increase its bandwidth such that $\tilde{q}$ converges to a sufficiently small value within the minimum dwell time. Therefore, the disturbance of τ in (13) could diminish between every two switchings by of $\psi(\tau_R) = 0$ and $\psi(\tau_R) \neq 0$. For $t \in [0, T]$ where $T > 0$ could be chosen arbitrarily, there are finite switchings and the $\mathcal{L}_2$ norm of the disturbance of τ could be bounded by a small value. By the finite-gain $\mathcal{L}_2$ stability proved in [14], the $\mathcal{L}_2$ norm of $\tilde{\theta}$ for $t \in [0, T]$ is also bounded by a small value. Since $\ddot{\theta}$ is bounded by (14a) and $\ddot{\theta}_d$ is bounded by Assumption 2, $\ddot{\tilde{\theta}}$ is also bounded. $\tilde{\theta}$ could therefore be bounded by a small value when its $\mathcal{L}_2$ norm is bounded for $t \in [0, T]$.

C. Implementation of the Proposed Controller

To implement the control law (11), it is necessary to compute $\dot{q}_d$ and $\ddot{q}_d$, it is mentioned in [3] that $\dot{q}_d$ and $\ddot{q}_d$ could be computed analytically without higher-order derivatives of θ, $\dot{\theta}$, q, $\dot{q}$. However, the computation is tedious and requires actual dynamics parameters of (3). To resolve this issue, the following third-order sliding mode differentiator [15] is applied to estimate $\dot{q}_d, \ddot{q}_d$.

$$\begin{aligned}
\dot{z}_0 &= -\tilde{\lambda}_3 L^{\frac{1}{4}} |z_0 - f(t)|^{\frac{3}{4}} \operatorname{sign}(z_0 - f(t)) + z_1 \\
\dot{z}_1 &= -\tilde{\lambda}_2 L^{\frac{2}{4}} |z_0 - f(t)|^{\frac{2}{4}} \operatorname{sign}(z_0 - f(t)) + z_2 \\
\dot{z}_2 &= -\tilde{\lambda}_1 L^{\frac{3}{4}} |z_0 - f(t)|^{\frac{1}{4}} \operatorname{sign}(z_0 - f(t)) + z_3 \\
\dot{z}_3 &= -\tilde{\lambda}_0 L \operatorname{sign}(z_0 - f(t))
\end{aligned} \tag{15}$$

where $f(t)$ is the input signal, L is the Lipschitz constant of $f^{(4)}(t)$, i.e., $\left|f^{(4)}(t)\right| \leq L$ holds. According to the theorem in [15], there exist $\tilde{\lambda}_i$ $(i = 0, 1, 2, 3)$ such that the differentiator can achieve $z_i(t) \to f^{(i)}(t)$ in finite time. By setting $f(t) = q_d$, we could obtain $z_1 \to \dot{q}_d$ and $z_2 \to \ddot{q}_d$. Since the sliding mode differentiator is third-order, the estimated $\dot{q}_d, \ddot{q}_d$ are both continuous.

One challenge of implementing the proposed controller is to keep $|\tau| < \tau_m$. In (14a), τ is controlled in an open-loop manner since only $\theta, \dot{\theta}, q, \dot{q}$ are available for the controller and no joint torque or cable tension information are used. The cable-loop controller (11) could achieve $\tau \to \sigma(\tau_R)$ only when $\tilde{q} \to 0$ and l could be accurately estimated by (1). However, for real CDMs, it is tedious to model accurate $f_{kin}(\theta)$ analytically since the cable routing is not the same as the ideal case illustrated in Figure 1. Instead, only nominal $\overline{f_{kin}}$ and $\overline{\partial_\theta l}$ are available for controller implementation. Thus, q_d in (12) is modified as

$$q_d = \frac{1}{\rho}\left(\frac{\sigma(\tau_R)}{2k\left(-\overline{\partial_\theta l}\right)}\right) + \overline{f_{kin}}(\theta). \tag{16}$$

By (1), (16), substitute q in (1) with $\tilde{q} + q_d$ and τ in (10a) now becomes

$$\tau = \frac{(\partial_\theta l)}{\left(\overline{\partial_\theta l}\right)}\sigma(\tau_R) - (\partial_\theta l)\, 2k\rho\left(\overline{f_{kin}}(\theta) - f_{kin}(\theta) + \tilde{q}\right). \tag{17}$$

Both $\overline{f_{kin}}$ and $\overline{\partial_\theta l}$ would cause extra disturbance on τ. In practice, τ is not sensitive to the error between $\overline{\partial_\theta l}$ when we use the ideal configuration in Figure 1 to derive $\overline{\partial_\theta l}$:

$$\overline{\partial_\theta l} = -nd\cos\frac{\theta}{2}. \tag{18}$$

The second term in (17) is a part of disturbance on τ. Since $|\partial_\theta l|$ is high due to the tension amplification design of LIMS elbow mechanism, the disturbance of τ would be exacerbated by error of $\overline{f_{kin}}$. To address this issue, a heuristic procedure is designed to improve the accuracy of $\overline{f_{kin}}$.

We perform two slow joint motion tests on the LIMS elbow CDM under varying load conditions: 1) no load is equipped; 2) a known load is equipped. By sending the motor a low-speed motion command, two sets of data of $(q_m,\ \theta)$ could be obtained, where q_m is the motor raw position feedback in a coordinate with an unknown offset compared with q. As θ strictly increases with q_m, two different continuous mappings $q_{m,i} = \eta_i(\theta)$, $i = 1, 2$ could be obtained by linear interpolation. i is the subscript for the two tests. Since $f_{kin}(\theta)$ is defined such that $l = 0$ always

holds, i.e., $\tau = 0$, it is necessary to estimate a mapping $q_{m,0} = \eta_0(\theta)$ when $l = 0$ and $\tau = 0$. Thus, the effect of $g(\theta)$ should be compensated. $\partial_q \tau(\theta)$ could be estimated by $\overline{\partial_q \tau}(\theta) = \frac{\tau_2(\theta)-\tau_1(\theta)}{q_{m,2}(\theta)-q_{m,1}(\theta)}$, where $\tau_1(\theta)$ and $\tau_2(\theta)$ are joint torque for the two tests. $\tau_2 - \tau_1$ could be calculated by the known load's mass and the elbow link's geometric parameters. Next, by the nominal elbow link's dynamics parameter, we could get $\bar{g}(\theta)$. $\eta_0(\theta)$ could then be obtained by $\eta_0(\theta) = \eta_1(\theta) - \left(\overline{\partial_q \tau}(\theta)\right)^{-1} \bar{g}(\theta)$. Finally, since $q = 0$ when $\theta = 0$, $\overline{f_{kin}}$ is defined as $\overline{f_{kin}}(\theta) = \eta_0(\theta) - \eta_0(0)$. Filtering could be applied to improve smoothness of $\overline{f_{kin}}$ which may help improve performance of motion control.

The zero position of $\overline{f_{kin}}$ may be calibrated to further reduce its constant offset error. For the proposed controller with $\theta_d(t) = 0$ and bounded τ_m, since τ is limited after $\sigma(\tau_R)$ is saturated, it is not sufficient to maintain $\theta_d(t) = 0$ when external torque reaches a certain level. We first apply enough force on the elbow link to move it slightly away from $\theta = 0$ in one direction and then maintain it in static state for a while. Next, the same procedure is repeated for the opposite joint direction. By comparing $|u|$ when the link is stopped, the offset for $\overline{f_{kin}}$ could be adjusted and the procedure could be repeated until $|u|$ are the same for both directions. The idea of the test is that $|\tau|$ should be the same for $\sigma(\tau_R) = \tau_m$ and $\sigma(\tau_R) = -\tau_m$ when $\tilde{q} = 0$. Since range of θ is small during the motion, $\partial_\theta l$ is almost constant. By (10), $|u|$ of the two cases should also be the same when the system is static.

To improve the robustness of the constraint $|\tau| < \tau_m$, a nominal $\bar{k}$ could also be introduced in (16):

$$q_d = \frac{1}{\rho}\left(\frac{\sigma(\tau_R)}{2\bar{k}\left(-\overline{\partial_\theta l}\right)}\right) + \overline{f_{kin}}(\theta). \tag{19}$$

In this way, the joint torque in (17) becomes

$$\tau = \frac{k(\partial_\theta l)}{\bar{k}\left(\overline{\partial_\theta l}\right)}\sigma(\tau_R) - (\partial_\theta l)\, 2k\rho\left(\overline{f_{kin}}(\theta) - f_{kin}(\theta) + \tilde{q}\right). \tag{20}$$

In practice, error of $\overline{f_{kin}}$ and $\tilde{q}$ could become disturbance for τ, which makes it more difficult to keep $|\tau| < \tau_m$. A simple strategy to improve its robustness is to use a larger $\bar{k}$ than cable's actual stiffness k. As a result, the first term in (20) could be bounded by $\pm\tau_m$, and the constraint $|\tau| < \tau_m$ would be more robust. On the other hand, increasing $\bar{k}$ may degrade the motion control performance. When the second term of (20) is zero, $\tau \approx k\bar{k}^{-1}\sigma(\tau_R)$ if we ignore the disturbance caused by $\overline{\partial_\theta l}$. In this way, $\tilde{\theta}$ would still converge to 0 when the right-hand side of (6) is replaced with $k\bar{k}^{-1}\sigma(\tau_R)$ thanks to the adaptive design of τ_R in (8). However, Assumption 2 should be modified such that $|\tau_d| < k\bar{k}^{-1}\tau_m$, which is more stringent than $|\tau_d| < \tau_m$. Therefore, there is a tradeoff between the robustness of the constraint $|\tau| < \tau_m$ and motion control performance when designing $\bar{k}$.

IV. Experimental Results and Discussions

The proposed controller is implemented in the real hardware to evaluate its capabilities in both joint tracking and constraining joint torque. We use a Maxon RE35 brushed motor with 21:1 gear reducer, and an Elmo Golden Solo Twitter as the drive for the motor. A JinGang MPT encoder with 24-bit resolution per cycle is installed on the joint to obtain position feedback and two Simba Touch tension sensors with 0.01N resolution are equipped to measure the cable tensions. The tension data is not used in the controller and is only used for experimental analysis. A C++ program is implemented in one computer with Ubuntu system to run the joint loop controller and update q_d. A ZLG EtherCATNET Ethercat master with 1ms cycle time is used to run cable-loop controller and also enables low-latency communication between the computer and Elmo drive. The sample rate of joint loop implemented in the computer is about 1000Hz. Cyclic synchronous position mode with position, velocity and torque offset inputs is implemented in the Elmo drive with 10kHz sample rate. The assembled elbow mechanism similar to LIMS [2] is shown in Figure 4. F_p is adjusted for the two cables such that $F_1 = 18N$ and $F_2 = 30N$ when $\theta = 0$. The cable stiffness k is around 30 N/mm . By observing cable slack deformation and analyzing cable tensions data, we set $F_0 = 10$N. Kinematics and dynamics parameters of the mechanism are shown in Appendix.

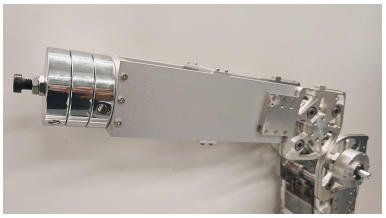

Fig. 4: The Elbow Mechanism for experiments with 1.5kg Load.

We design five experiments to verify the effectiveness of the proposed controller:

1) Joint tracking with different loads.
2) Joint tracking of small-amplitude but fast trajectories.
3) Step trajectory response.
4) Compliant motion.
5) Stop the joint motion by a fixed small wooden stick.

Experiments 1) and 2) mainly aim to verify the joint tracking performance of the proposed controller. The controller is expected to demonstrate good performance under varying load and speed conditions thanks to the adaptive design in joint-loop controller. Experiments 3)-5) focus on evaluating the effect of the safety joint torque constraint. In Experiment 3), θ_d is designed as step-type to show whether the torque constraint is satisfied during fast and abrupt movements. In Experiment 4), we drag the elbow link to test its motion compliance with the proposed controller and assess if the torque constraint remains valid under external torque disturbances. Finally, in Experiment 5), a fixed wooden stick is used as an obstacle to test if the elbow link could be stopped to satisfy the torque constraint.

Two other baseline controllers are used in comparison with the proposed controller: (8), (9), (11), and (19). The first one is a PID controller which also has a joint loop and cable loop

like Figure 2. The joint-loop controller is

$$\tau_{PID}(t) = -K_p\tilde{\theta} - K_d\dot{\tilde{\theta}} - K_i\int_0^t \tilde{\theta}(\tau)\,d\tau. \tag{21}$$

The cable-loop controller is (11) without the compensation term $\rho(2kl)$:

$$u_{PID} = -K_1\tilde{q} - K_2\dot{\tilde{q}} + J_\rho\ddot{q}_\mathrm{d}. \tag{22}$$

The calculation of q_d for PID controller is similar to (19) except $\sigma(\tau_R)$ is replaced by τ_{PID}.

The other is a kinematics controller which does not have a joint loop and ignores the flexibility of actuator-to-joint transmission. The controller is same as (22) but q_d is calculated by

$$q_d = \overline{f_{kin}}(\theta_d). \tag{23}$$

The control parameters for the proposed controller are tuned empirically as follows : $A = 766.6$, $B = 9.43$, $\alpha = 100$, $\bar{k} = 46\,\mathrm{N/mm}$, $P = \mathrm{diag}(0.94, 2.35, 47.18)$, K_1 = 213.3, K_2 = 1.06, $J_\rho = 1.5\times10^{-4}\mathrm{kg.m}^2$. τ_m is to be specified for different experiments. The initial value of $\hat{p}$ for the joint-loop controller could be calculated based on nominal parameters shown in the appendix, and they differ significantly from true dynamic parameters of the system. The parameters for the third-order sliding mode differentiator are: $L = 5\times10^4$, $\tilde{\lambda}_0$ to $\tilde{\lambda}_3$ are 1.1, 3.06, 4.16, 3, respectively. Additionally, $\dot{q}_d$ is filtered using a low-pass filter with time constant 25ms. For PID controller, $K_p = 943.59$, $K_d = 11.79$, $K_i = 1179.50$. These parameters are tuned to balance tracking accuracy and motion smoothness. K_1 and K_2, third-order differentiator and low-pass filter parameters are same as the proposed controller for both PID and kinematics controllers.

In Experiment 1), the desired joint trajectory is $\theta_d = \frac{\pi}{12} + \frac{\pi}{8}\left(1 - \cos\frac{\pi t}{18}\right)$. The initial position is $\theta_0 = \frac{\pi}{12}$ and the total motion time is 18 seconds. The load conditions are no load, 0.7kg, and 1.5kg. $\tau_m = 13.8$Nm is set for the proposed controller and the saturation of $\sigma(\tau_R)$ does not happen throughout the experiment. As shown in Table I, the proposed controller has the lowest mean absolute error (MAE) for all load conditions compared with other two controllers. PID controller has lower MAE compared to kinematics controller because the joint loop is more robust to cable deformation caused by various loads.

TABLE I: MAE (degree) of $\tilde{\theta}$ for Experiment 1).

Controller	0kg	0.7kg	1.5kg
Proposed	0.010	0.012	0.015
PID	0.033	0.038	0.047
Kinematics	0.094	0.120	0.238

In Experiment 2), a 0.7kg load is always attached to the link's end. $\theta_d = \frac{\pi}{36} - \frac{\pi}{36}\sin(\omega t)$ and three tests with ω = 2π/s, 3π/s, and 4π/s for three controllers are conducted. $\tau_m = 13.8$Nm is set for the proposed controller in this experiment. The tracking error is shown in Figure 5. Results

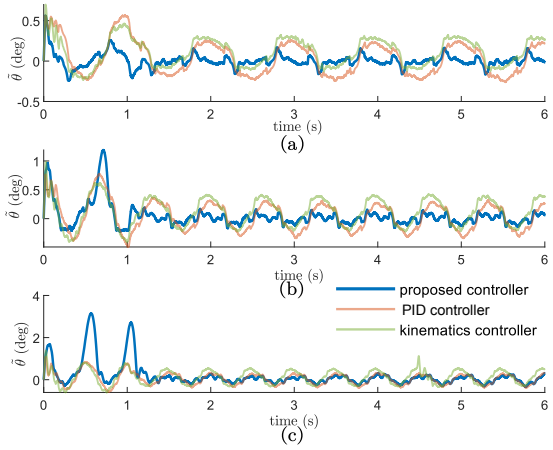

Fig. 5: $\tilde{\theta}$ of Experiment 2). (a) $\omega = 2\pi$/s. (b) $\omega = 3\pi$/s. (c) $\omega = 4\pi$/s.

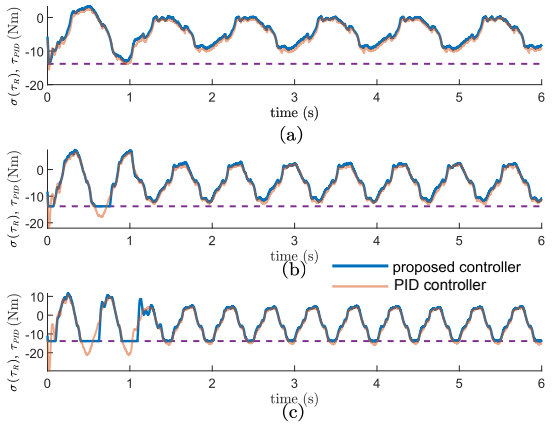

Fig. 6: $\sigma(\tau_R)$ and τ_{PID} for Experiment 2). Purple dashed line: $-\tau_m$. (a) $\omega = 2\pi$/s. (b) $\omega = 3\pi$/s. (c) $\omega = 4\pi$/s.

of joint loop controller τ_R and τ_{PID} are shown in Figure 6. MAE results are shown in Table II. Ranges of $\hat{\tau}$ are as Table III. The joint torque is calculated using cable tensions' data by $\hat{\tau} = -(\bar{\partial}_\theta \bar{l})(F_1 - F_2)$. By the tracking error result, the proposed controller has the lowest MAE for $\omega = 2\pi$/s and 3π/s. However, for $\omega = 4\pi$/s, MAE of the proposed controller is slightly higher than the PID controller. This is because $\tilde{\theta}$ is higher from $t = 0s$ to $1.8s$ for the proposed controller as shown in Figure 5(c). During this period in Figure 6(c), τ_R reaches the bound $-\tau_m$ and becomes saturated several times, which limits the joint torque and joint speed. Therefore, there is a tradeoff between improving tracking accuracy and constraining joint torque. From $t = 1.8s$ to $6s$, $\tilde{\theta}$ for the three controllers are approximately periodic and our controller still has lower MAE 0.120 degree compared with 0.194 degree of PID controller. Moreover, $\hat{\tau}$ of the proposed controller does not go lower than -3.57Nm for all three tests. $\hat{\tau}$ of the other two controllers reach more negative values compared with the proposed controller when $\omega = 3\pi/s$ and $4\pi/s$. The minimal cable tensions for the two controllers are below $F_0 = 10N$ and around 9N when $\omega =$

TABLE II: MAE (degree) of $\tilde{\theta}$ for Experiment 2).

Controller	$\omega = 2\pi$/s	$\omega = 3\pi$/s	$\omega = 4\pi$/s	$\omega = 4\pi$/s (t=1.8 to 6s)
Proposed	0.055	0.110	0.270	0.112
PID	0.185	0.221	0.234	0.194
Kinematics	0.168	0.230	0.300	0.273

TABLE III: Range of $\hat{\tau}$ (Nm) for Experiment 2).

Controller	$\omega = 2\pi$/s	$\omega = 3\pi$/s	$\omega = 4\pi$/s
Proposed	[-3.42, -2.47]	[-3.49, -2.08]	[-3.57, -0.18]
PID	[-3.40, -2.52]	[-3.93, -2.09]	[-4.65, -0.93]
Kinematics	[-3.44, -2.31]	[-3.99, -1.84]	[-4.58, -0.75]

$4\pi/s$, while the proposed controller's is 10.65N for all three tests. This illustrates the proposed controller's advantage in limiting joint torque and alleviating cable slack phenomenon.

In Experiment 3), the elbow link is equipped with a 0.7kg load and $\tau_m = 13.8$Nm for the proposed controller. θ_d is step-type and each time the joint is commanded to move 2 degrees. As shown in Figure 7, θ has less overshoot and range of $\hat{\tau}$ is smaller for the proposed controller. In Figure 8a, $\sigma(\tau_R)$ is also saturated as expected each time the joint moves rapidly to limit τ. The minimal cable tension is 11.08N for the proposed controller, and below $F_0 = 10N$ around 9.08N for PID controller. This again highlights the capability of the proposed controller in mitigating cable slack phenomenon.

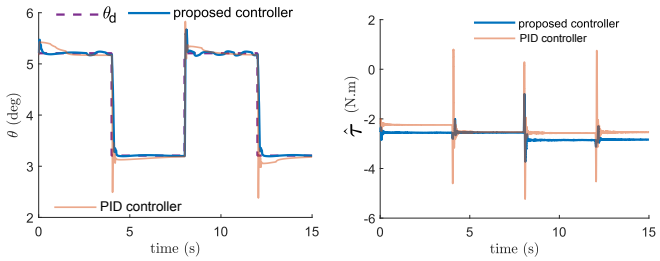

(a) (b)

Fig. 7: Data of θ and $\hat{\tau}$ for Experiment 3). (a) Tracking performance comparison. (b) $\hat{\tau}$ comparison.

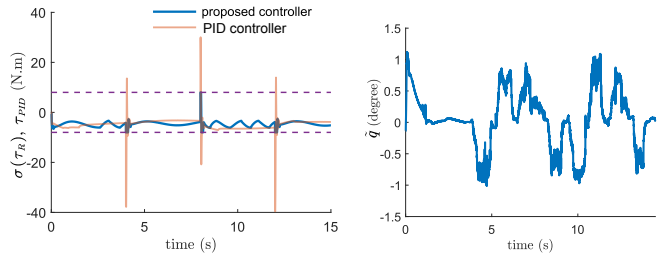

(a) (b)

Fig. 8: (a) $\sigma(\tau_R)$ and τ_{PID} for Experiment 3). Purple dashed line: $\pm\tau_m$ (b) $\tilde{q}$ for Experiment 4) when $\tau_m = 3$Nm.

In Experiment 4), we set $\theta_d = 0$ and conduct compliant motion tests for the proposed controller with $\tau_m = 3$Nm, 5Nm, and 7Nm to see if $|\hat{\tau}| < \tau_m$ could be maintained. Results of $\theta, \tilde{\theta}$, and $\hat{\tau}$ are shown in Figure 9 and Figure 8b. We set $\theta(0) = 0$ and $\theta_d(t) = 0$. The elbow link's end is dragged to move accordingly. As shown in Figure 9, the joint moves away from $\theta_d = 0$ in both directions. This is because when $\sigma(\tau_R)$ is saturated, τ is limited by $\pm\tau_m$ and it is not sufficient to counter the external torque. In Figure 9, $\hat{\tau}$ when $\tau_m = 5$Nm and 7Nm is always within the bounds. But when $\tau_m = 3$Nm, $\hat{\tau}$ sometimes goes slightly out of bounds . This could be explained by the limited motor position bandwidth as shown in Figure 8b, where the max magnitude of $\tilde{q}$ is about 1 degree. It would lead to disturbance about 1.8Nm in τ by (14a), which increases the difficulty of keeping $|\tau| < \tau_m$ when τ_m is low. Thanks to the design of $\bar{k} > k$ in (19), $\hat{\tau}$ does not exceed the constraint when $\tau_m = 5$Nm and 7Nm in the presence of torque disturbance caused by $\tilde{q}$.

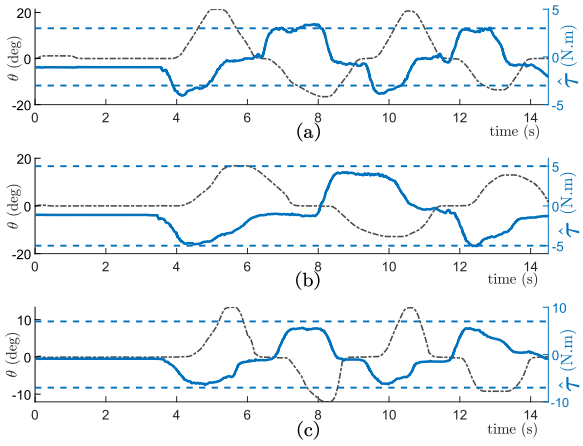

Fig. 9: θ and $\hat{\tau}$ for Experiment 4). Black dash-dotted line: θ. Blue line: $\hat{\tau}$. Blue dashed line: $\pm\tau_m$. (a) $\tau_m = 3$Nm. (b) $\tau_m = 5$Nm. (c) $\tau_m = 7$Nm.

In Experiment 5), we use a fixed wooden stick cut from a coffee stirrer to stop the joint motion. We set $\theta_d = \frac{23\pi}{180} - \frac{\pi}{18}\left(1 - \cos\frac{2\pi}{9}t\right)$ and $\tau_m = 5.7$Nm. The max force on the stick's free could bear before cracking is about 1.2N to 3N. Two photos are shown as Figure 11. Results of θ and $\hat{\tau}$ are shown in Figure 10a. During t = 2-6s and 12-15s, the link contacts with the wooden stick and the proposed controller stops joint motion and $\hat{\tau}$ remains at about -2.1Nm. For PID controller, the joint keeps moving when contacting with the stick and $\hat{\tau}$ quickly goes to -2.5Nm in Figure 10b. The stick thus breaks as shown in Figure 11b during t = 2-3s. This experiment further illustrates the effectiveness of our proposed controller in torque constraints satisfaction.

V. Conclusion

In this paper, a novel controller is proposed for flexible LIMS elbow CDM. A dynamic model for LIMS elbow CDM is introduced at first. It considers cable flexibility and model the relationship among joint torque, motor and joint position. Then an anti-windup adaptive controller for traditional manipulators is briefly reviewed. Next, we propose the hierarchical adaptive controller with configurable joint torque

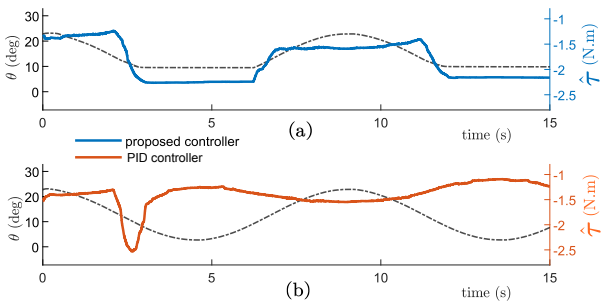

Fig. 10: θ and $\hat{\tau}$ for Experiment 5). Black dash-dotted line: θ. Blue line: $\hat{\tau}$ for the proposed controller. Orange line: $\hat{\tau}$ for the PID controller.

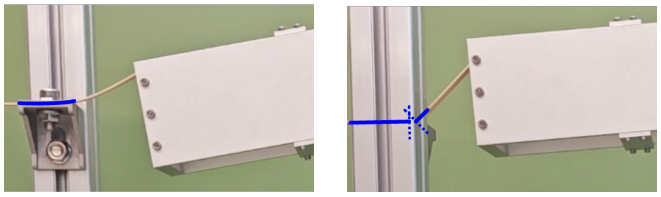

(a) (b)

Fig. 11: Photos of Experiment 5). (a) Stick stops the elbow link with the proposed controller. (b) Stick breaks with PID controller. Blue line: hidden part of the stick.

constraints and briefly analyze its stability. Implementation details including estimation of derivatives of motor desired position and calibration of actuator-to-joint kinematics are discussed in details. Finally, several experiments have been conducted to validate the effectiveness of the proposed controller in joint tracking, limiting joint torque, and reducing cable slack.

Future works could focus on extending the controller design and implementation for CDMs with multiple degrees of freedom, where inter-joint coupling in cable routing would pose extra challenges to the estimation of cable deformation via actuator-to-joint kinematics. Another direction is to design algorithms to further improve the robustness of constraining joint torque under limited motor bandwidth while maintaining motion control performance.

APPENDIX

$$J(\theta) = J_c + m\left(\frac{1}{4}h^2 + e^2 + he\cos\frac{\theta_a}{2}\right)$$
$$C(\theta,\dot{\theta}) = -\frac{1}{4}mhe\sin\left(\frac{\theta_a}{2}\right)\dot{\theta}$$
$$g(\theta) = -mg\left(e\cos\theta + \frac{1}{2}h\sin\left(\frac{\theta_a}{2}\right)\right)$$

where $\theta_a = \theta + \frac{\pi}{2}$, m is the total mass of the elbow link, J_c is the constant inertia of the elbow link about the center of mass, e is the distance between the elbow link's center of mass and the center of the circular part, and h is the diameter of the elbow link's circular part.

$Y(\theta,\dot{\theta},\dot{\theta},\ddot{\theta})$ and p in (8) are formulated as the following:

$$Y(\theta,\dot{\theta},\dot{\theta},\ddot{\theta}) =$$
$$\begin{bmatrix} h\cos\frac{\theta_a}{2}\ddot{\theta} - \frac{1}{4}h\sin\frac{\theta_a}{2}\dot{\theta}^2 - g\cos\theta & \frac{1}{4}h^2\ddot{\theta} - \frac{1}{2}gh\sin\frac{\theta_a}{2} & \ddot{\theta} \end{bmatrix}$$
$$p = \begin{bmatrix} me & m & me^2 + J_c \end{bmatrix}^T.$$

For the experimental mechanism, the parameters are: $d =$ 31mm, $h =$ 80mm, $n =$4, $\rho =$17mm, $e =$ 94mm, $J_c =$ 0.01kg.m^2, $m =$ 1.07kg. The distance from the elbow link's end surface to the center of its rolling circular part is 244mm. Nominal dynamics parameters are $\bar{J}_c = 0.1\text{kg.m}^2$, $\bar{e}$ = 100mm, and $\bar{m}$ = 0.4kg.

REFERENCES

[1] T. Lens and O. Von Stryk, "Design and dynamics model of a lightweight series elastic tendon-driven robot arm," in *2013 IEEE International Conference on Robotics and Automation*. Karlsruhe, Germany: IEEE, May 2013, pp. 4512–4518.

[2] Y.-J. Kim, "Anthropomorphic Low-Inertia High-Stiffness Manipulator for High-Speed Safe Interaction," *IEEE Transactions on Robotics*, vol. 33, no. 6, pp. 1358–1374, Dec. 2017.

[3] B. Brogliato, R. Ortega, and R. Lozano, "Global tracking controllers for flexible-joint manipulators: A comparative study," *Automatica*, vol. 31, no. 7, pp. 941–956, July 1995.

[4] L. Le-Tien and A. Albu-Schaffer, "Robust Adaptive Tracking Control Based on State Feedback Controller With Integrator Terms for Elastic Joint Robots With Uncertain Parameters," *IEEE Transactions on Control Systems Technology*, vol. 26, no. 6, pp. 2259–2267, Nov. 2018.

[5] T. V. Trung and M. Iwasaki, "Fast and Precise Positioning With Coupling Torque Compensation for a Flexible Lightweight Two-Link Manipulator With Elastic Joints," *IEEE/ASME Transactions on Mechatronics*, vol. 28, no. 2, pp. 1025–1036, Apr. 2023.

[6] M. Miyasaka, M. Haghighipanah, Y. Li, J. Matheson, A. Lewis, and B. Hannaford, "Modeling Cable-Driven Robot With Hysteresis and Cable–Pulley Network Friction," *IEEE/ASME Transactions on Mechatronics*, vol. 25, no. 2, pp. 1095–1104, Apr. 2020.

[7] J. D. S. B. Neto, W. Li, S. Togo, H. Yokoi, and Y. Jiang, "Model-Based Tension And State Estimation For Sensorless Joints Tendon-Driven Mechanisms," in *2024 International Conference on Advanced Robotics and Mechatronics (ICARM)*. Tokyo, Japan: IEEE, July 2024, pp. 106–112.

[8] E. Sariyildiz, H. Wang, and H. Yu, "A sliding mode controller design for the robust position control problem of series elastic actuators," in *2017 IEEE International Conference on Robotics and Automation (ICRA)*. Singapore, Singapore: IEEE, May 2017, pp. 3055–3061.

[9] K. Choi, J. Kwon, T. Lee, C. Park, J. Pyo, C. Lee, S. Lee, I. Kim, S. Seok, Y.-J. Kim, and F. C. Park, "A hybrid dynamic model for the AMBIDEX tendon-driven manipulator," *Mechatronics*, vol. 69, p. 102398, Aug. 2020.

[10] Y. Wang, S. Li, D. Wang, F. Ju, B. Chen, and H. Wu, "Adaptive Time-Delay Control for Cable-Driven Manipulators With Enhanced Nonsingular Fast Terminal Sliding Mode," *IEEE Transactions on Industrial Electronics*, vol. 68, no. 3, pp. 2356–2367, Mar. 2021.

[11] J. Ma, Y. Li, and S. S. Ge, "Adaptive control for a cable driven robot arm," in *2012 IEEE International Conference on Mechatronics and Automation*. Chengdu, China: IEEE, Aug. 2012, pp. 1074–1079.

[12] J. Kirchhoff and O. Von Stryk, "Robust trajectory tracking control for an ultra lightweight tendon driven series elastic robot arm," in *2016 IEEE International Conference on Advanced Intelligent Mechatronics (AIM)*. Banff, AB, Canada: IEEE, July 2016, pp. 1297–1304.

[13] C. Song and D. Lau, "Workspace-Based Model Predictive Control for Cable-Driven Robots," *IEEE Transactions on Robotics*, vol. 38, no. 4, pp. 2577–2596, Aug. 2022.

[14] M. Kanamori, "Finite-gain L2 stability of anti-windup adaptive tracking control for Euler-Lagrange systems with actuator saturation," in *2014 IEEE International Conference on Robotics and Automation (ICRA)*. Hong Kong, China: IEEE, May 2014, pp. 2495–2500.

[15] Y. Shtessel, C. Edwards, L. Fridman, and A. Levant, *Sliding Mode Control and Observation*, ser. Control Engineering. New York, NY: Springer New York, 2014.